Available online at www.sciencedirect.com
ScienceDirect
Journal of Sound and Vibration 317 (2008) 158–174
JOURNAL OF SOUND AND VIBRATION
www.elsevier.com/locate/jsvi

Identification of the dynamic properties of joints using frequency–response functions

Damjan Čelič, Miha Boltežar*

Faculty of Mechanical Engineering, University of Ljubljana, Aškerčeva 6, SI-1000 Ljubljana, Slovenia

Received 30 January 2008; received in revised form 14 February 2008; accepted 4 March 2008
Handling Editor: C.L. Morfey

Abstract

The dynamic properties of joints are extremely difficult to model accurately using a purely analytical approach. However, these properties can be extracted from experimental data. In this paper we present a method for establishing a theoretical model of a joint from the substructures and assembly frequency–response function (FRF) data. The identification process considers not only translational, but also rotational degrees of freedom (RDOFs). The validity of the proposed method is demonstrated numerically and experimentally. A combined numerical–experimental approach was used to identify the mass, stiffness and damping effects of a real bolted joint. Using the least-squares method, data from the wide frequency range were used. A substructure synthesis method with the joint effects included was used to check the extracted values.

1. Introduction

Many mechanical structures are composed of substructures connected together by joints such as bolts, rivets, glue and welds. The main purpose of joint identification is to estimate the parameters of the joint that minimize the difference between the measured assembly response characteristics and those predicted analytically or numerically [1]. In the past few years, the numerical techniques used for structural dynamic problems, such as the FEM, have made a lot of progress. However, the unmodeled variability in the joint's properties and the boundary conditions, as well as the unmodeled nonlinearities, are the main reasons for the uncertainty of the finite-element (FE) models. Alternatively, the joint's properties can also be extracted from measured data.

To identify the joint's structural parameters, measured modal parameters have been used in several studies. These methods require accurate modal data, which are difficult to extract, especially in cases of closely coupled and heavily damped modes [2].

In order to overcome the difficulties encountered when extracting accurate modal parameters, several attempts were made to identify the joint's properties from the measured substructure frequency–response

*Corresponding author. Tel.: +386 1 4771 608; fax: +386 1 2518 567.
E-mail address: miha.boltezar@fs.uni-lj.si (M. Boltežar).

0022-460X/$ - see front matter © 2008 Elsevier Ltd. All rights reserved.
doi:10.1016/j.jsv.2008.03.009

functions (FRFs) and the joint-dependent FRFs of the whole structure using a least-squares method. Tsai and Chou [3] proposed a method to identify the dynamic characteristics of a single bolt joint. Ren and Beards [4] generalized the FRF joint-identification technique for systems involving multiple rigid and flexible joints. They extracted the joint's parameters from the experimental data and established a theoretical model of a joint. The dynamic stiffness matrix of the joint was constructed using mass, stiffness, viscous and/or structural damping matrices. An effort was made to reduce the effect of the measurement errors by introducing a proper criterion for the best solution. Another identification method for linear joint models based on Ren's method was developed by Liu [5]. A robustness investigation of the proposed algorithms was also carried out.

However, an FRF measurement at a joint is usually not possible, so FRF-based identification methods also face some difficulties. Yang and Park [2] combined incomplete measured FRFs with the substructure FE model, which excludes the undetermined joint properties. The unmeasured FRFs were estimated by solving an over-determined set of linear equations derived from measured FRFs and the FE model of the substructures. By assuming a model of the joint, the joint's structural parameters were extracted from measured and estimated FRFs using an iterative output error algorithm.

Some investigations considered only translational degrees of freedom (TDOFs), while the rotational DOFs (RDOFs) were taken into consideration using two closely separated TDOFs [3–6]. In some cases, when the substructures are separated by a nut, two TDOFs on the contact area can represent the joint's properties up to a certain high frequency [3]. Unfortunately, this is not always the case in reality, so such formulations are not sufficient.

A joint can also be modeled using a set of translational and rotational springs [2,7], but in this case the cross-coupled terms between the TDOFs and RDOFs are not considered.

The full consequences and errors caused by excluding RDOF data in joint-parameter identification and coupling analyses were not clearly understood in the past. Liu [5] investigated the impact of RDOF on joint-parameter identification and came to the conclusion that the information about RDOFs plays an important role in the identification process. However, from his work it is not clear how the RDOFs are included in the identification process.

Yang et al. [8] considered the model of a joint as a coupled stiffness matrix, instead of just a set of translational and rotational springs. Their method used an accurately calibrated FE model of the unconstrained structure to obtain the necessary information about the RDOFs. Next, a substructural synthesis method was used to identify the translational and rotational stiffness of the joint. The model of the joint was considered as a coupled stiffness matrix, instead of just a set of translational and rotational springs [8]. Unfortunately, their formulation includes many inverse operations and is therefore subjected to numerical errors. Furthermore, no damping was addressed in their paper.

In this paper an improved joint-identification method is presented. The method is based on that developed by Ren and Beards [4,6,7]. In contrast to the original method, where the effects of rotation were excluded, in our derivation not only the mass, stiffness and damping effects, but also the effects of rotation, are considered. The merit of this approach is that it handles the TDOFs and RDOFs in a clear and systematic way, which easily allows an expansion to more DOFs or to a larger number of joints. In order to make our identification method more suitable for experimental use, a new identification equation was also developed.

Following the example of Ren and Beards a joint-identification algorithm for the least-squares solution is also used. The feasibility of the proposed identification method is tested numerically and experimentally.

2. Identification of linear joints

Linear models of joints are mostly used for modeling tightly fastened joints, while nonlinear models normally exhibit friction-related nonlinearities. The load–deformation relationship in the normal direction becomes effectively linear after a pre-load and can be considered as linear in most applications, while the relationship in the tangential direction is always nonlinear and energy is dissipated when a cyclic load is applied [5]. In most engineering structures the friction joints are often tightly fastened so that their potential nonlinear behavior is suppressed and so it is not significant. The main concern of this paper is linear models of joints.

2.1. Theory

The identification of real joint parameters can only be carried out using experimental data. The most convenient way is to use FRFs, which can be measured directly. In our case, receptance data were used.

The basic strategy of most FRF joint-identification techniques is to measure the properties of a substructure system without joints and an assembly system with joints. The difference between the dynamic properties of the two cases is the result of the joints [1].

Consider a model with three systems: the first is the substructure system, the second is the joint system and the third is the assembly system, as shown in Fig. 1[4]. For the substructure system the coordinates are divided into joint and internal coordinates, with the subscripts b and a, respectively. The coordinates on the assembly are also divided into joint and internal coordinates, with the subscripts j and n, respectively. The joint system is represented by subscript c. Assuming no external moment acting on the coordinates a and n, $\mathbf{m}_a = 0$ and $\mathbf{m}_n = 0$, the relationship between the input and the output of the substructure can be expressed as

$$\begin{Bmatrix} \mathbf{x}_a \\ \mathbf{x}_b \\ \boldsymbol{\theta}_b \end{Bmatrix} = \begin{bmatrix} \mathbf{TT}_{aa} & \mathbf{TT}_{ab} & \mathbf{TR}_{ab} \\ \mathbf{TT}_{ba} & \mathbf{TT}_{bb} & \mathbf{TR}_{bb} \\ \mathbf{RT}_{ba} & \mathbf{RT}_{bb} & \mathbf{RR}_{bb} \end{bmatrix} \begin{Bmatrix} \mathbf{f}_a \\ \mathbf{f}_b \\ \mathbf{m}_b \end{Bmatrix}, \tag{1}$$

where $\mathbf{x}$, $\boldsymbol{\theta}$, $\mathbf{f}$ and $\mathbf{m}$ are the displacement, the angular displacement, the force and the moment, respectively. $\mathbf{TT}$, $\mathbf{TR}$, $\mathbf{RT}$ and $\mathbf{RR}$ are the frequency–response matrices corresponding to the TDOFs and RDOFs. For the internal coordinates (a), only TDOFs are considered, while for the joint coordinates (b), TDOFs and RDOFs are considered. The receptance matrices are denoted in the same way as in Ref. [8]. The relationship for the assembly is

$$\begin{Bmatrix} \mathbf{x}_n \\ \mathbf{x}_j \\ \boldsymbol{\theta}_j \end{Bmatrix} = \begin{bmatrix} \mathbf{TT}_{nn} & \mathbf{TT}_{nj} & \mathbf{TR}_{nj} \\ \mathbf{TT}_{jn} & \mathbf{TT}_{jj} & \mathbf{TR}_{jj} \\ \mathbf{RT}_{jn} & \mathbf{RT}_{jj} & \mathbf{RR}_{jj} \end{bmatrix} \begin{Bmatrix} \mathbf{f}_n \\ \mathbf{f}_j \\ \mathbf{m}_j \end{Bmatrix}. \tag{2}$$

The characteristics of the joint can be described by the dynamic stiffness matrix $\mathbf{Z}_j$,

$$\begin{Bmatrix} \mathbf{f}_c \\ \mathbf{m}_c \end{Bmatrix} = \mathbf{Z}_j \begin{Bmatrix} \mathbf{x}_c \\ \boldsymbol{\theta}_c \end{Bmatrix}; \quad \mathbf{Z}_j = \begin{bmatrix} \mathbf{Z}_{TT} & \mathbf{Z}_{TR} \\ \mathbf{Z}_{RT} & \mathbf{Z}_{RR} \end{bmatrix}. \tag{3}$$

The forces and displacements of the internal coordinates experience no change before and after the coupling

$$\mathbf{f}_a = \mathbf{f}_n \quad \text{and} \quad \mathbf{x}_a = \mathbf{x}_n. \tag{4}$$

The equilibrium and compatibility conditions at the joint coordinates must also be satisfied, therefore

$$\begin{Bmatrix} \mathbf{f}_b \\ \mathbf{m}_b \end{Bmatrix} + \begin{Bmatrix} \mathbf{f}_c \\ \mathbf{m}_c \end{Bmatrix} = \begin{Bmatrix} \mathbf{f}_j \\ \mathbf{m}_j \end{Bmatrix} \quad \text{and} \quad \begin{Bmatrix} \mathbf{x}_j \\ \boldsymbol{\theta}_j \end{Bmatrix} = \begin{Bmatrix} \mathbf{x}_b \\ \boldsymbol{\theta}_b \end{Bmatrix} = \begin{Bmatrix} \mathbf{x}_c \\ \boldsymbol{\theta}_c \end{Bmatrix}. \tag{5}$$

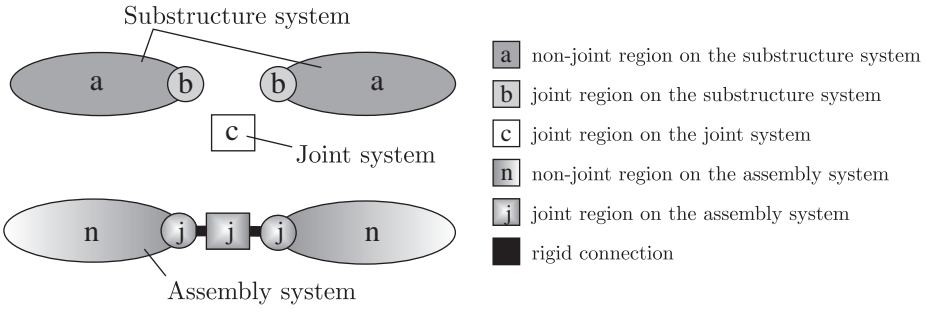

Fig. 1. Three systems in joint identification.

Substituting the compatibility and equilibrium conditions (4) and (5) into Eq. (1) gives

$$\begin{Bmatrix} \mathbf{x}_c \\ \boldsymbol{\theta}_c \end{Bmatrix} = \begin{Bmatrix} \mathbf{x}_b \\ \boldsymbol{\theta}_b \end{Bmatrix} = \begin{bmatrix} \mathbf{TT}_{ba} \\ \mathbf{RT}_{ba} \end{bmatrix} \mathbf{f}_a + \begin{bmatrix} \mathbf{TT}_{bb} & \mathbf{TR}_{bb} \\ \mathbf{RT}_{bb} & \mathbf{RR}_{bb} \end{bmatrix} \begin{Bmatrix} \mathbf{f}_b \\ \mathbf{m}_b \end{Bmatrix}. \tag{6}$$

Substituting the joint's characteristics (3) into Eq. (6), and considering equilibrium conditions at the joint's coordinates (5), the following equation is obtained:

$$\begin{Bmatrix} (\mathbf{f}_j - \mathbf{f}_b) \\ (\mathbf{m}_j - \mathbf{m}_b) \end{Bmatrix} = \mathbf{Z}_j \begin{Bmatrix} \mathbf{x}_c \\ \boldsymbol{\theta}_c \end{Bmatrix} = \mathbf{Z}_j \begin{bmatrix} \mathbf{TT}_{ba} \\ \mathbf{RT}_{ba} \end{bmatrix} \mathbf{f}_a + \mathbf{Z}_j \begin{bmatrix} \mathbf{TT}_{bb} & \mathbf{TR}_{bb} \\ \mathbf{RT}_{bb} & \mathbf{RR}_{bb} \end{bmatrix} \begin{Bmatrix} \mathbf{f}_b \\ \mathbf{m}_b \end{Bmatrix}. \tag{7}$$

Rearranging Eq. (7) leads to

$$\begin{Bmatrix} \mathbf{f}_b \\ \mathbf{m}_b \end{Bmatrix} = \left(\mathbf{I} + \mathbf{Z}_j \begin{bmatrix} \mathbf{TT}_{bb} & \mathbf{TR}_{bb} \\ \mathbf{RT}_{bb} & \mathbf{RR}_{bb} \end{bmatrix} \right)^{-1} \left(\begin{Bmatrix} \mathbf{f}_j \\ \mathbf{m}_j \end{Bmatrix} - \mathbf{Z}_j \begin{bmatrix} \mathbf{TT}_{ba} \\ \mathbf{RT}_{ba} \end{bmatrix} \mathbf{f}_a \right). \tag{8}$$

Rearranging, Eq. (1) can be written in the form

$$\begin{Bmatrix} \mathbf{x}_a \\ \mathbf{x}_b \\ \boldsymbol{\theta}_b \end{Bmatrix} = \begin{bmatrix} \mathbf{TT}_{aa} \\ \mathbf{TT}_{ba} \\ \mathbf{RT}_{ba} \end{bmatrix} \mathbf{f}_a + \begin{bmatrix} \mathbf{TT}_{ab} & \mathbf{TR}_{ab} \\ \mathbf{TT}_{bb} & \mathbf{TR}_{bb} \\ \mathbf{RT}_{bb} & \mathbf{RR}_{bb} \end{bmatrix} \begin{Bmatrix} \mathbf{f}_b \\ \mathbf{m}_b \end{Bmatrix}. \tag{9}$$

Using Eq. (8) and the compatibility conditions (4), (5) in Eq. (9), and comparing with the assembly characteristics (2), gives

$$\begin{bmatrix} \mathbf{TT}_{nn} \\ \mathbf{TT}_{jn} \\ \mathbf{RT}_{jn} \end{bmatrix} = \begin{bmatrix} \mathbf{TT}_{aa} \\ \mathbf{TT}_{ba} \\ \mathbf{RT}_{ba} \end{bmatrix} - \begin{bmatrix} \mathbf{TT}_{ab} & \mathbf{TR}_{ab} \\ \mathbf{TT}_{bb} & \mathbf{TR}_{bb} \\ \mathbf{RT}_{bb} & \mathbf{RR}_{bb} \end{bmatrix} \left(\mathbf{I} + \mathbf{Z}_j \begin{bmatrix} \mathbf{TT}_{bb} & \mathbf{TR}_{bb} \\ \mathbf{RT}_{bb} & \mathbf{RR}_{bb} \end{bmatrix} \right)^{-1} \mathbf{Z}_j \begin{bmatrix} \mathbf{TT}_{ba} \\ \mathbf{RT}_{ba} \end{bmatrix} \tag{10}$$

and

$$\begin{bmatrix} \mathbf{TT}_{nj} & \mathbf{TR}_{nj} \\ \mathbf{TT}_{jj} & \mathbf{TR}_{jj} \\ \mathbf{RT}_{jj} & \mathbf{RR}_{jj} \end{bmatrix} = \begin{bmatrix} \mathbf{TT}_{ab} & \mathbf{TR}_{ab} \\ \mathbf{TT}_{bb} & \mathbf{TR}_{bb} \\ \mathbf{RT}_{bb} & \mathbf{RR}_{bb} \end{bmatrix} \left(\mathbf{I} + \mathbf{Z}_j \begin{bmatrix} \mathbf{TT}_{bb} & \mathbf{TR}_{bb} \\ \mathbf{RT}_{bb} & \mathbf{RR}_{bb} \end{bmatrix} \right)^{-1}. \tag{11}$$

Finally, substituting Eq. (11) into Eq. (10) leads to equations for the identification of the dynamic stiffness matrix of the joint $\mathbf{Z}_j$ ($N \times N$)

$$\begin{bmatrix} \mathbf{TT}_{nn} \\ \mathbf{TT}_{jn} \\ \mathbf{RT}_{jn} \end{bmatrix} = \begin{bmatrix} \mathbf{TT}_{aa} \\ \mathbf{TT}_{ba} \\ \mathbf{RT}_{ba} \end{bmatrix} - \begin{bmatrix} \mathbf{TT}_{nj} & \mathbf{TR}_{nj} \\ \mathbf{TT}_{jj} & \mathbf{TR}_{jj} \\ \mathbf{RT}_{jj} & \mathbf{RR}_{jj} \end{bmatrix} \mathbf{Z}_j \begin{bmatrix} \mathbf{TT}_{ba} \\ \mathbf{RT}_{ba} \end{bmatrix} \tag{12}$$

or

$$\begin{bmatrix} \mathbf{TT}_{aa} - \mathbf{TT}_{nn} \\ \mathbf{TT}_{ba} - \mathbf{TT}_{jn} \\ \mathbf{RT}_{ba} - \mathbf{RT}_{jn} \end{bmatrix} = \begin{bmatrix} \mathbf{TT}_{nj} & \mathbf{TR}_{nj} \\ \mathbf{TT}_{jj} & \mathbf{TR}_{jj} \\ \mathbf{RT}_{jj} & \mathbf{RR}_{jj} \end{bmatrix} \mathbf{Z}_j \begin{bmatrix} \mathbf{TT}_{ba} \\ \mathbf{RT}_{ba} \end{bmatrix}. \tag{13}$$

Distinguishing between the joint and non-joint coordinates is very convenient in this case. It should be stressed that the coordinates of the joint are fixed, while the non-joint coordinates can be chosen more freely.

Unfortunately, the FRF matrices relating to the joint coordinates and the RDOFs are not always possible to measure. However, in most cases the necessary information about RDOFs for unconstrained substructures can be obtained from the accurately calibrated FE model. However, in order to identify the real joint parameters, FRFs of the assembly need to be measured.

Obviously, Eq. (13) is not very convenient for practical use. In order to overcome this problem, an alternative form of the identification (Eq. (13)) was developed

$$\begin{bmatrix} \mathbf{TT}_{aa}-\mathbf{TT}_{nn} \\ \mathbf{TT}_{ba}-\mathbf{TT}_{jn} \\ \mathbf{RT}_{ba}-\mathbf{RT}_{jn} \end{bmatrix} = \left\{ \begin{bmatrix} \mathbf{TT}_{ab} & \mathbf{TR}_{ab} \\ \mathbf{TT}_{bb} & \mathbf{TR}_{bb} \\ \mathbf{RT}_{bb} & \mathbf{RR}_{bb} \end{bmatrix} - \begin{bmatrix} \mathbf{TT}_{aa}-\mathbf{TT}_{nn} \\ \mathbf{TT}_{ba}-\mathbf{TT}_{jn} \\ \mathbf{RT}_{ba}-\mathbf{RT}_{jn} \end{bmatrix} \cdot \begin{bmatrix} \mathbf{TT}_{ba} \\ \mathbf{RT}_{ba} \end{bmatrix}^{+} \begin{bmatrix} \mathbf{TT}_{bb} & \mathbf{TR}_{bb} \\ \mathbf{RT}_{bb} & \mathbf{RR}_{bb} \end{bmatrix} \right\} \mathbf{Z}_j \begin{bmatrix} \mathbf{TT}_{ba} \\ \mathbf{RT}_{ba} \end{bmatrix}, \tag{14}$$

where $[]^{+}$ stands for the generalized or pseudo-inverse [9]. The derivation of Eq. (14) is given in Appendix A.

Using Eq. (14), only the receptance matrices $\mathbf{TT}_{nn}$, $\mathbf{TT}_{jn}$ and $\mathbf{RT}_{jn}$ need to be measured, while all the other receptance matrices can be obtained from the substructure FE models. The matrix $\mathbf{TT}_{nn}$ refers to non-joint coordinates and can easily be measured. It is a little more complicated to measure the $\mathbf{TT}_{jn}$ matrix, where the responses have to be measured at the joint coordinates. However, measuring the $\mathbf{RT}_{jn}$ matrix is the most difficult task. The latter can only be measured by using special rotational transducers.

Another possibility for solving this problem is to use the equation

$$[\mathbf{TT}_{aa}-\mathbf{TT}_{nn}] = \left\{ [\mathbf{TT}_{ab} \;\; \mathbf{TR}_{ab}] - [\mathbf{TT}_{aa}-\mathbf{TT}_{nn}] \cdot \begin{bmatrix} \mathbf{TT}_{ba} \\ \mathbf{RT}_{ba} \end{bmatrix}^{+} \begin{bmatrix} \mathbf{TT}_{bb} & \mathbf{TR}_{bb} \\ \mathbf{RT}_{bb} & \mathbf{RR}_{bb} \end{bmatrix} \right\} \mathbf{Z}_j \begin{bmatrix} \mathbf{TT}_{ba} \\ \mathbf{RT}_{ba} \end{bmatrix}, \tag{15}$$

which is a truncated form of Eq. (14). In this case only the $\mathbf{TT}_{nn}$ matrix needs to be measured. Although this is a very convenient method, there is still a major drawback: important information about the system is lost.

The third option is to estimate the unmeasured FRFs by solving an over-determined set of linear equations derived from measured FRFs and the substructure FE model [2]. If the number of measured FRFs is greater than or equal to that of the joint-related DOFs, then, according to Yang and Park [2], the unmeasured FRFs can be estimated using the following equation:

$$\{\mathbf{h}_{\mathrm{est}}(\omega)\} = [\mathbf{D}_{be}(\omega)]^{+}(\{\mathbf{I}_{lb}\} - [\mathbf{D}_{bm}(\omega)]\{\mathbf{h}_m(\omega)\}), \tag{16}$$

where $\{\mathbf{h}_m(\omega)\}$ is the measured FRF column vector, $\{\mathbf{h}_{\mathrm{est}}(\omega)\}$ is the FRF column vector to be estimated, and $\mathbf{D}_{bm}(\omega)$ and $\mathbf{D}_{be}(\omega)$ are the known dynamic stiffness matrices of the substructure system.

2.2. Joint-identification algorithm

Eqs. (13)–(15) all have the general form

$$\mathbf{C}_{(M\times L)} = \mathbf{A}_{(M\times N)}\mathbf{Z}_{j\,(N\times N)}\mathbf{B}_{(N\times L)}, \tag{17}$$

where $\mathbf{A}$, $\mathbf{B}$ and $\mathbf{C}$ are coefficient matrices and M, N and L represent the size of the corresponding matrix. If $M, L \geqslant N$ and the matrices $\mathbf{A}$ and $\mathbf{B}$ are nonsingular, Eq. (17) becomes determined or over-determined and $\mathbf{Z}_j$ can be solved uniquely [4,10]. The least-squares solution of Eq. (17) is

$$\mathbf{Z}_j = \mathbf{A}^{+}\mathbf{C}\mathbf{B}^{+}, \tag{18}$$

where the superscript plus sign denotes the pseudo-inverse of the matrix. Eq. (17) can also be re-written as a set of linear equations

$$\mathbf{E}(\omega)\mathbf{z}(\omega) = \mathbf{g}(\omega), \tag{19}$$

where $\mathbf{z}$ is a frequency-dependent $N^2 \times 1$ vector whose elements are constructed from $\mathbf{Z}_j$ [4]. $\mathbf{E}$ is the coefficient matrix constructed from matrices $\mathbf{A}$ and $\mathbf{B}$, and $\mathbf{g}$ is a coefficient vector constructed from the matrix $\mathbf{C}$. Ren

and Beards [4] also introduced a linear transformation to convert the vector **z** into a frequency-independent vector **x**

$$\mathbf{z}(\omega) = \mathbf{T}_f \mathbf{x}, \tag{20}$$

using a transformation matrix

$$\mathbf{T}_f = \left[\mathbf{I} \quad -\frac{\omega^2}{\omega_0^2}\mathbf{I} \quad \mathrm{i}\frac{\omega}{\omega_0}\mathbf{I} \quad \mathrm{i}\mathbf{I}\right], \tag{21}$$

where ω_0 is a reference angular frequency, which is usually equal to the maximum measured frequency [4]. Vector **x** is formed in terms of the mass, the stiffness and the damping matrices as follows:

$$x = \{\mathbf{k} \quad \omega_0^2\mathbf{m} \quad \omega_0\mathbf{c} \quad \mathbf{d}\}^{\mathrm{T}}. \tag{22}$$

The substitution of Eq. (20) into Eq. (19) yields

$$\mathbf{E}(\omega)\mathbf{T}_f\mathbf{x} = \mathbf{g}(\omega). \tag{23}$$

Since the vector **x** is frequency independent, Eq. (23) at different frequencies can be combined directly, and the solution in the sense of least squares can be found [10]

$$\mathbf{x} = \left[\sum_{i=1}^{n}[(\mathbf{E}(\omega))^{\mathrm{T}}\mathbf{E}(\omega)]^{-1}\sum_{i=1}^{n}((\mathbf{E}(\omega))^{\mathrm{T}}\mathbf{g}(\omega))\right]. \tag{24}$$

Identified elements of the mass, the stiffness and the damping matrices are then constant values, which are valid across the whole selected frequency range.

Although this solution is quite useful from the theoretical point of view, there are some difficulties in its practical usage. With the identification of real joints, some nonlinearities, measurement noise and numerical errors are inevitably present. In this case the vector **x** becomes frequency dependent and its least-squares solution is incorrect. By finding the solution of Eq. (23) for each particular frequency, an indication of the system's nonlinearities and error effects can be given.

If the system is lightly damped, the magnitude of the FRFs at the resonant frequencies will be much higher than that at the other frequencies. Consequently, although all the measured data are used at the same time, the results are dominated by the data at just a few frequency points [10]. To improve the results the data at different frequencies and at different coordinates should be properly weighted. Different weighting techniques are discussed in Refs. [4,10].

Choosing a proper frequency range and the correct number of frequency points is also essential to the accuracy of the identification. It is not the total number of equations, but the number of effective equations that is important in the identification. A sufficiently wide frequency range and sufficiently well-spaced coordinates should be measured [10]. It is generally believed that the effects of measurement errors can be significantly magnified at resonance frequencies, and therefore they should be excluded in the identification process [4,8,10].

3. Case studies

In order to check the feasibility of the proposed identification method, numerical and experimental work was carried out. A numerical example and an experimental case are presented. The numerical example deals with the multiple degree of freedom (MDOF) system on a purely analytical basis.

3.1. Numerical case study 1

The proposed method was verified on a simple linear MDOF mass–spring system with six TDOFs (x_1-x_6) and six RDOFs ($\phi_1-\phi_6$), as shown in Fig. 2. The 12 DOF system is treated as an assembly composed of a

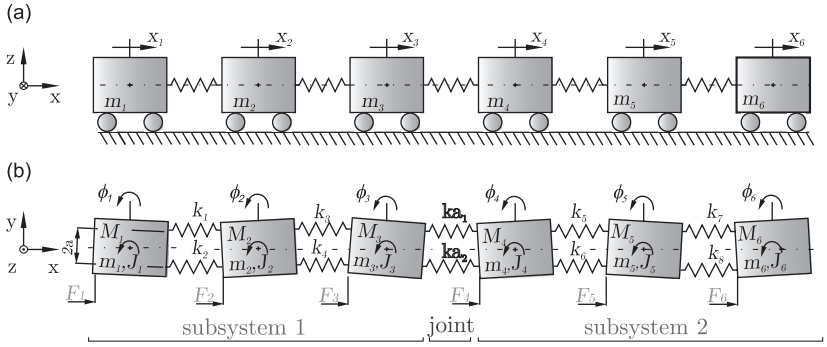

Fig. 2. MDOF mass–spring system; (a) front view, (b) top view; m represents mass and M is the external momentum.

Table 1
Input data of MDOF system

Index	Mass, m (kg)	Mass moment of inertia, J (kg m^2)	Stiffness, k (N m^{-1})	Moment arm, a (m)
1	3	0.7	$3 \cdot 10^6$	0.05
2	1	0.5	$5 \cdot 10^7$	0.05
3	2	0.6	$1 \cdot 10^8$	0.05
4	1	0.2	$5 \cdot 10^6$	0.05
5	2	0.6	$3 \cdot 10^7$	0.05
6	1.5	0.4	$7 \cdot 10^6$	0.05
7	–	–	$2 \cdot 10^7$	–
8	–	–	$1 \cdot 10^6$	–

joint and two subsystems. The joint is represented by two translational springs with stiffness coefficients ka_1 and ka_2. Since no mass and damping effects are included in the joint, the model of the joint can be considered just in terms of the stiffness matrix

$$\mathbf{Z}_j = \begin{bmatrix} \mathbf{K}_{TT} & \mathbf{K}_{TR} \\ \mathbf{K}_{RT} & \mathbf{K}_{RR} \end{bmatrix}. \tag{25}$$

Assuming infinitesimal rotations, a simple analytical solution for the MDOF system can be found. Table 1 shows the selected input data for the MDOF system. By changing the values of the stiffness coefficients ka_1 and ka_2, more or less flexible joints can be simulated and the effectiveness of the identification procedure can be tested.

Using the theory of MDOF systems, substructure and assembly FRFs were calculated. After that the joint parameters $\mathbf{Z}_j$ were identified using Eq. (14) and the joint-identification algorithm (Section 2.2). For selected values of the stiffness coefficients $ka_1 = 10^{10}$ N m^{-1} and $ka_2 = 10^{11}$ N m^{-1} the identified dynamic stiffness matrix of the joint had the form

$$\mathbf{Z}_j = \begin{bmatrix} 1.1000 & -1.1000 & -0.0450 & 0.0450 \\ -1.1000 & 1.1000 & 0.0450 & -0.0450 \\ -0.0450 & 0.0450 & 0.0028 & -0.0028 \\ 0.0450 & -0.0450 & -0.0028 & 0.0028 \end{bmatrix} \cdot 10^{11}. \tag{26}$$

In order to check the influence of errors on the identification results, the dynamic stiffness matrix of the joint $\mathbf{Z}_j$ was identified at each particular frequency. According to the assumed model, our system is completely linear, and therefore the identified elements of the stiffness matrix should be constant values.

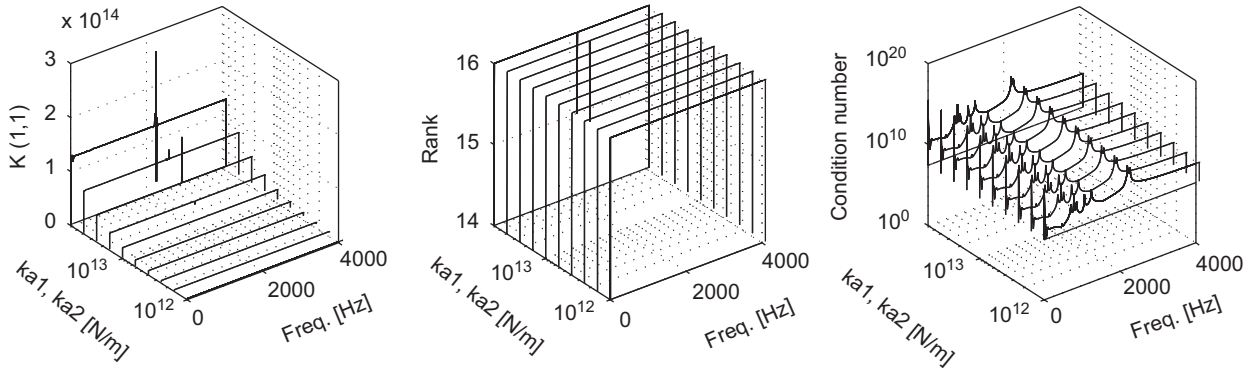

Fig. 3. The result of the joint identification at each individual frequency point for various stiffness coefficients $ka_1 = ka_2$; rank and condition number of a matrix product $\mathbf{E}(\omega)\mathbf{T}_f$ from Eq. (23) vs. stiffness coefficients $ka_1 = ka_2$ and frequency.

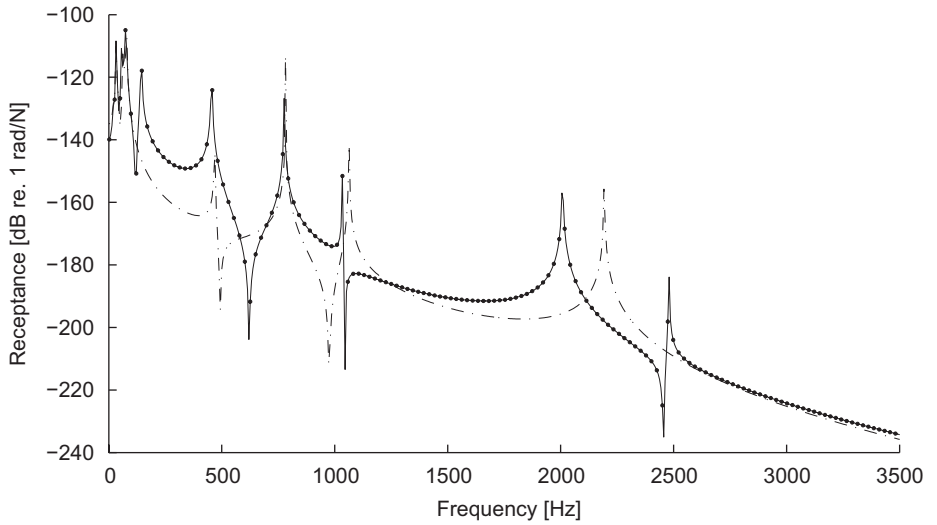

Fig. 4. Comparison of FRFs for $ka_1 = 10^8\,\mathrm{N\,m^{-1}}$ and $ka_2 = 10^7\,\mathrm{N\,m^{-1}}$. • $\mathbf{RT}_{jn}(1,1)$—exact, — $\mathbf{RT}_{jn}(1,1)$—reconstructed, – · – $\mathbf{RT}_{jn}(1,1)$—rigid coupling.

Fig. 3 shows the element $\mathbf{K}(1,1)$ of the identified stiffness matrix $\mathbf{K}_{TT}$ as a function of the frequency and stiffness coefficients $ka_1 = ka_2$. At a sufficiently low level of the stiffness coefficients, i.e., $ka_1 = ka_2 = 10^{12}\,\mathrm{N\,m^{-1}}$, the identified $\mathbf{K}_{TT}$ is approximately constant within the selected frequency range. However, by increasing ka_1 and ka_2 more discrepancies appear and $\mathbf{K}_{TT}$ becomes frequency dependent.

Fig. 3 also shows the rank and the condition number of the matrix product $\mathbf{E}(\omega)\mathbf{T}_f$ from Eq. (23) as a function of the frequency and stiffness coefficients. In the plot of $\mathbf{K}(1,1)$ some discrepancies (peaks) are seen at $ka_1 = ka_2 > 2 \cdot 10^{13}\,\mathrm{N\,m^{-1}}$ and at approximately 2 kHz. Also, the plots of the rank and the condition number resemble erroneous behavior at the same frequency; the rank falls from full rank (16) to 15, and the condition number is the highest exactly in that area. From Fig. 3 it is clear, that the bad identification results are a consequence of the system's ill-conditioning.

From the identified parameters of the joint and the noise-free FRFs of the substructures, the assembly FRFs were reconstructed. The quality of the identification can be visualized by comparing the exact and the reconstructed assembly FRFs.

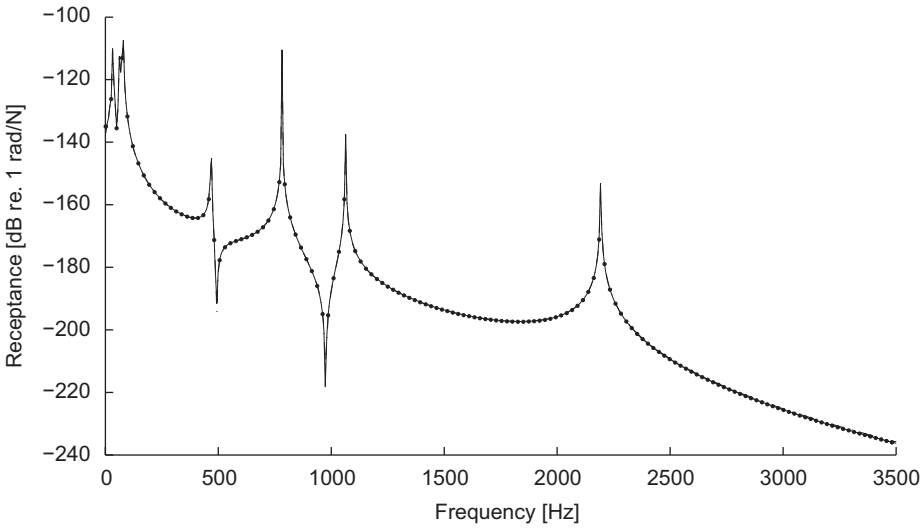

Fig. 5. Comparison of FRFs for $ka_1 = 10^8\,\mathrm{N\,m^{-1}}$ and $ka_2 = 10^7\,\mathrm{N\,m^{-1}}$. • $\mathbf{RT}_{jn}(1,1)$—exact, — $\mathbf{RT}_{jn}(1,1)$—reconstructed, – · – $\mathbf{RT}_{jn}(1,1)$—rigid coupling.

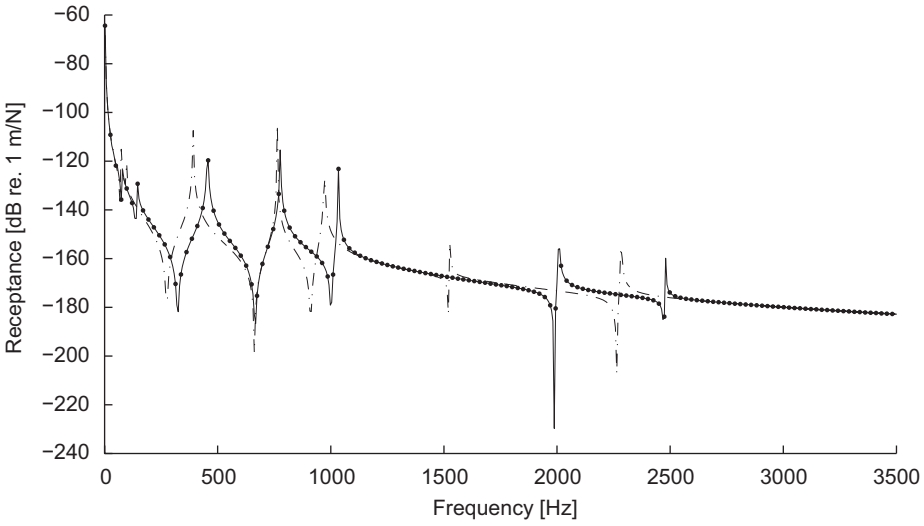

Fig. 6. Comparison of FRFs for $ka_1 = 10^8\,\mathrm{N\,m^{-1}}$ and $ka_2 = 10^7\,\mathrm{N\,m^{-1}}$. • $\mathbf{TT}_{nn}(1,1)$—exact, — $\mathbf{TT}_{nn}(1,1)$—reconstructed—TDOFs and RDOFs, – · – $\mathbf{TT}_{nn}(1,1)$—reconstructed—TDOFs.

Figs. 4 and 5 show the results of the identification for the soft and stiff joints, respectively. Very good agreement between the exact and reconstructed receptance curves was obtained in both cases (Figs. 4 and 5). In other words, our identification theory performs very well with the noise-free data.

The dash–dot lines in Figs. 4 and 5 represent the rigid coupling of the substructures [10–13]. If the joint is stiff enough, the limit state, i.e., a rigid connection, is achieved. This is the case in Fig. 5. It must be stressed that the receptance $\mathbf{RT}_{jn}$ relates to the RDOFs and TDOFs. It appears that the dash–dot curve and the solid curve in Fig. 5 are exact fit.

If the RDOFs are excluded in the identification process, important information about the system is lost. For the system in Fig. 2, the influence of considering the RDOFs on the identification results is illustrated in Fig. 6. The dashed curve in Fig. 6 represents the identification result in the case when only TDOFs were taken into

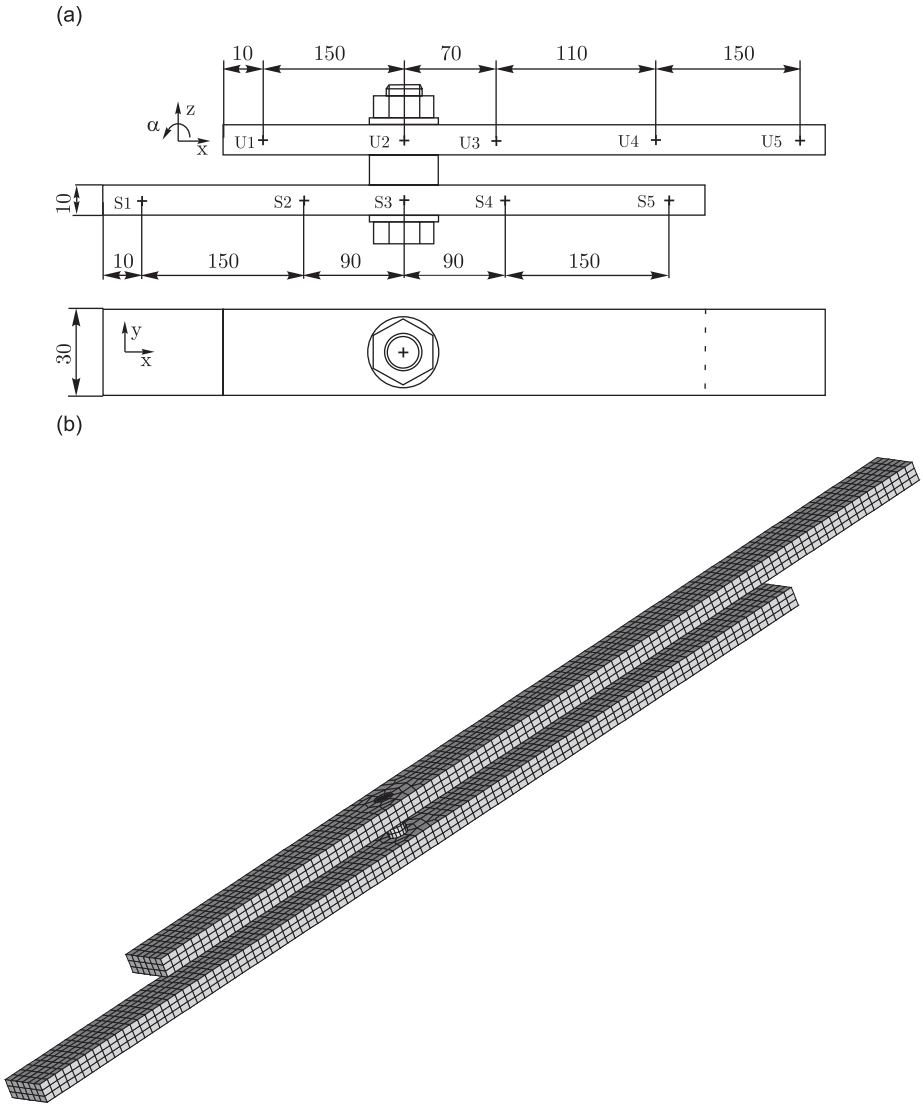

Fig. 7. (a) Real assembly and (b) finite-element model.

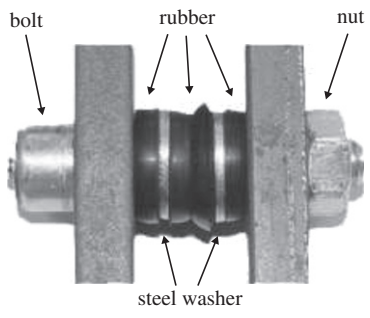

Fig. 8. Joint composition.

consideration, while the solid line represents the result of the identification theory including the RDOFs. It is evident that considering only TDOFs is not sufficient for the identification of the joint.

3.2. Experimental case study

The test assembly consisted of two parallel steel beams with the same rectangular cross section, 29×10 mm, and a length of 500 mm, which were connected together by an elastic joint, as shown in Fig. 7(a). The joint consisted of a bolt, rubber and steel washers, as shown in Fig. 8.

An electrodynamic shaker was used to measure the substructure and the assembly FRFs (Fig. 9). The measurements were made at five coordinates on each substructure, which results in 10 coordinates on the assembly, as shown in Fig. 7(a). The measured accelerance data were converted to receptance data by multiplying the accelerance by $-1/\omega^2$.

The structure was suspended in such a manner that it could vibrate only in one translational direction and one rotational direction (z and α in Fig. 7(a)). The joint was assumed to have two TDOFs ($U2_z$, $S3_z$) and two RDOFs ($U2_\alpha$, $S3_\alpha$). Consequently, the dynamic stiffness matrix of the joint had the form

$$\mathbf{Z}_j = \begin{bmatrix} U2_z/U2_z & U2_z/S3_z & U2_z/U2_\alpha & U2_z/S3_\alpha \\ S3_z/U2_z & S3_z/S3_z & S3_z/U2_\alpha & S3_z/S3_\alpha \\ U2_\alpha/U2_z & U2_\alpha/S3_z & U2_\alpha/U2_\alpha & U2_\alpha/S3_\alpha \\ S3_\alpha/U2_z & S3_\alpha/S3_z & S3_\alpha/U2_\alpha & S3_\alpha/S3_\alpha \end{bmatrix} = \begin{bmatrix} \mathbf{Z}_{TT} & \mathbf{Z}_{TR} \\ \mathbf{Z}_{RT} & \mathbf{Z}_{RR} \end{bmatrix}.$$

Using the available equipment (Fig. 9) only FRF data related to TDOFs were measured. An example of a measured FRF is shown in Fig. 10. Unfortunately, the identification of the dynamic stiffness matrix of the joint $\mathbf{Z}_j$ using Eq. (13) or Eq. (14) could not be made without FRF data related to the RDOFs. This was the main obstacle in the identification process.

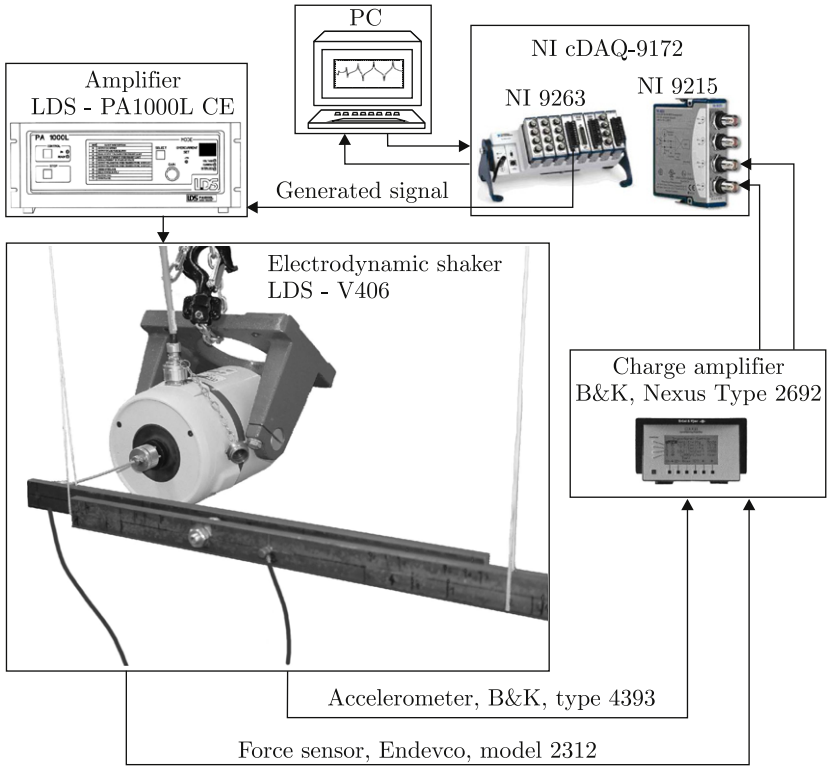

Fig. 9. FRF measurement using electrodynamic shaker.

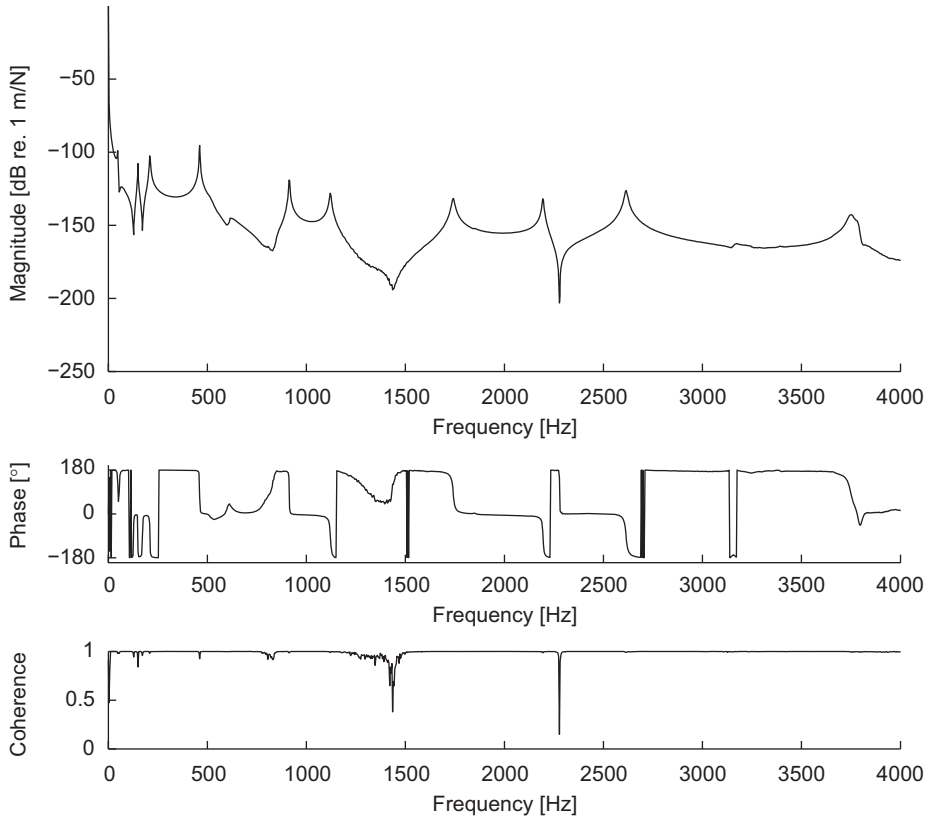

Fig. 10. Measured assembly FRF ($S3_z/U4_z$).

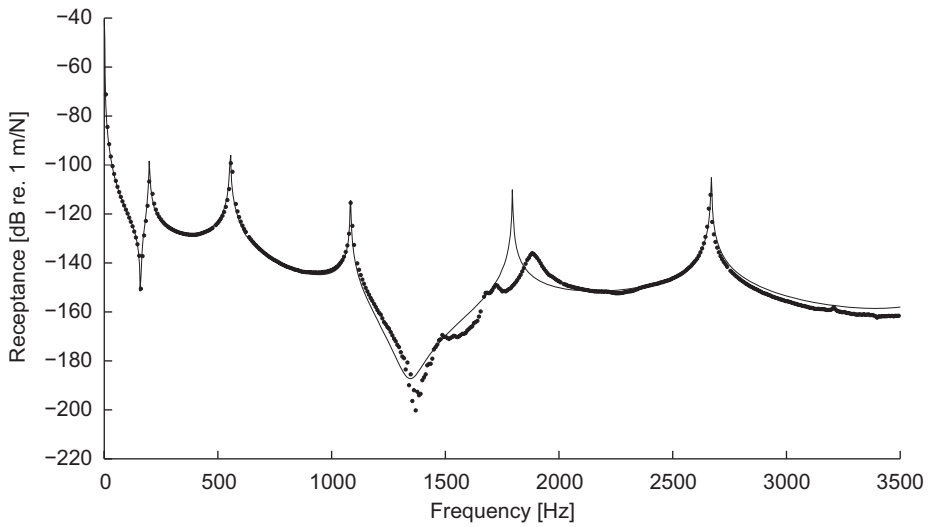

Fig. 11. Comparison of FRFs for symmetric beam ($S2_z/S4_z$). • Measured, — MKE.

Instead of measuring RDOFs, which is a very difficult task, unmeasured FRFs were estimated from the substructure FE model without a joint (Fig. 7(b)) and measured FRFs using Eq. (16). In order to do this the substructure FE models had to be accurately calibrated.

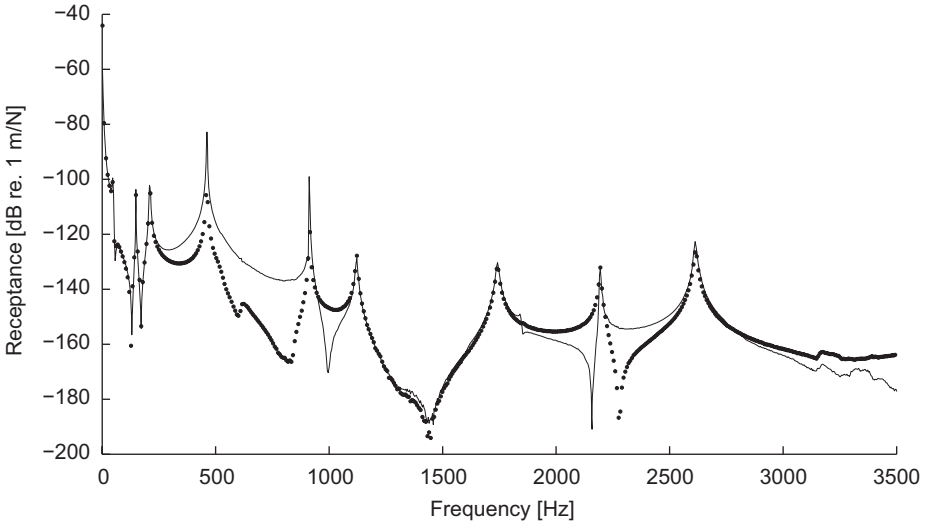

Fig. 12. Comparison of joint-related FRFs ($S3_z/U4_z$). • Measured, — estimated.

Receptance data were calculated from the modal data [9]. For each substructure 150 modes of vibration were used, which covers the frequency range up to 58 kHz, and for the assembly 300 modes of vibration were used, which covers the frequency range up to 47 kHz. A comparison of the measured and calculated FRFs for a symmetric beam is shown in Fig. 11. Since measuring FRFs at the joint's coordinates is not always possible, joint-related FRFs were also estimated. A comparison of the measured and estimated joint-related assembly FRFs is shown in Fig. 12.

Partly measured and partly estimated FRFs were used for the joint identification and to predict the assembly FRFs. Apparently, if the joint properties are accurately identified, the response of the assembly must be accurately predicted from the substructure FRFs and the identified joint parameters. The model of the joint was considered in terms of the mass, stiffness and hysteretic damping matrices

$$\mathbf{Z}_j = \begin{bmatrix} \mathbf{K}_{TT} & \mathbf{K}_{TR} \\ \mathbf{K}_{RT} & \mathbf{K}_{RR} \end{bmatrix} - \omega^2 \begin{bmatrix} \mathbf{M}_{TT} & \mathbf{M}_{TR} \\ \mathbf{M}_{RT} & \mathbf{M}_{RR} \end{bmatrix} + \mathrm{i} \begin{bmatrix} \mathbf{D}_{TT} & \mathbf{D}_{TR} \\ \mathbf{D}_{RT} & \mathbf{D}_{RR} \end{bmatrix}. \tag{27}$$

As already stated in Ref. [5], it is very important how many and which internal DOFs are used to achieve an acceptable result. The number of internal DOFs should at least be equal to the number of unknown joint parameters. From the simulations, the specific selection of four TDOFs ($S1_z$, $S2_z$, $U1_z$, $U4_z$) and two RDOFs ($S1_\alpha$, $S2_\alpha$) as internal DOFs gave the best result.

3.2.1. Results of the joint identification

Two identification procedures were performed. In first case, the dynamic stiffness matrix of the joint $\mathbf{Z}_j$ was calculated for each individual frequency point, using Eq. (14). This solution is denoted as the direct solution. The identified element of the dynamic stiffness matrix $\mathbf{Z}_j(1,1)$ is shown in Fig. 13. Based on the identified joint data and the substructure FRFs the assembly FRFs were regenerated (Fig. 14). The results of the identification are very good in the frequency range from 0 to 900 Hz. However, some discrepancies appear at higher frequencies.

In the second case, using Eq. (14) the least-squares solution (Eq. (24)) for the dynamic stiffness matrix of the joint $\mathbf{Z}_j$ was performed. In order to avoid inaccurate results the frequency points included in the identification process had to be properly selected. Following the example from the numerical case study, the condition number of the matrix product $\mathbf{E}(\omega)\mathbf{T}_f$ from Eq. (23) was used as a measure for selecting the frequency points. In our case, the frequency-selection criterion was

$$\mathrm{cond}(\mathbf{E}(\omega)\mathbf{T}_f) < 5 \cdot 10^{19}.$$

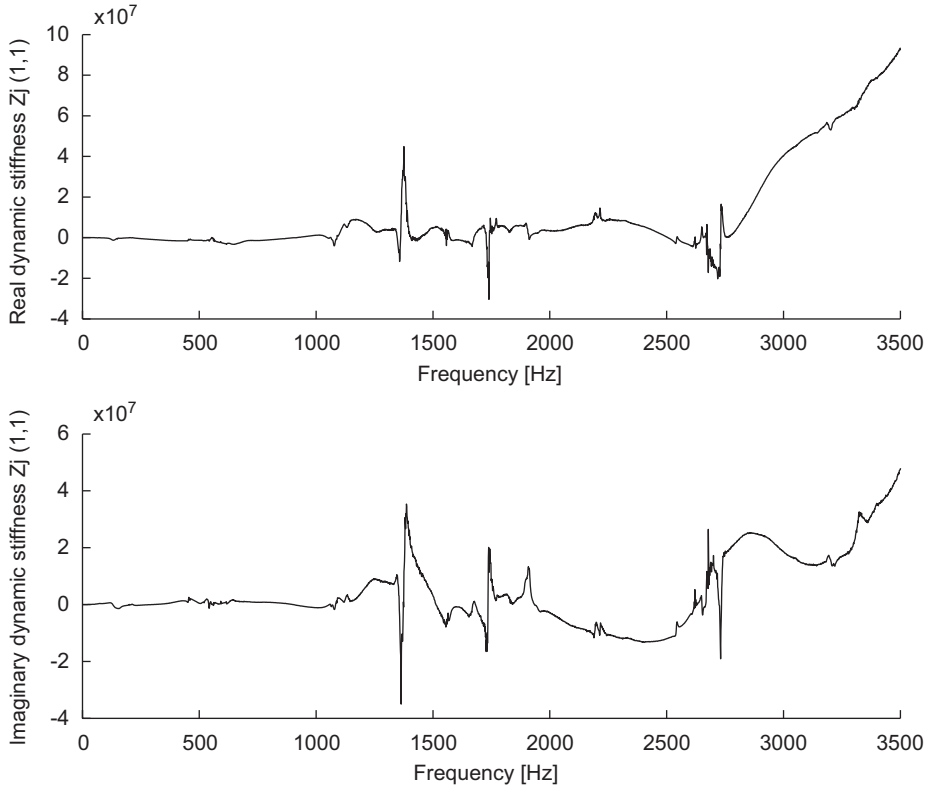

Fig. 13. Identified dynamic stiffness $\mathbf{Z}_j(1,1)$ at each individual frequency point using Eq. (14).

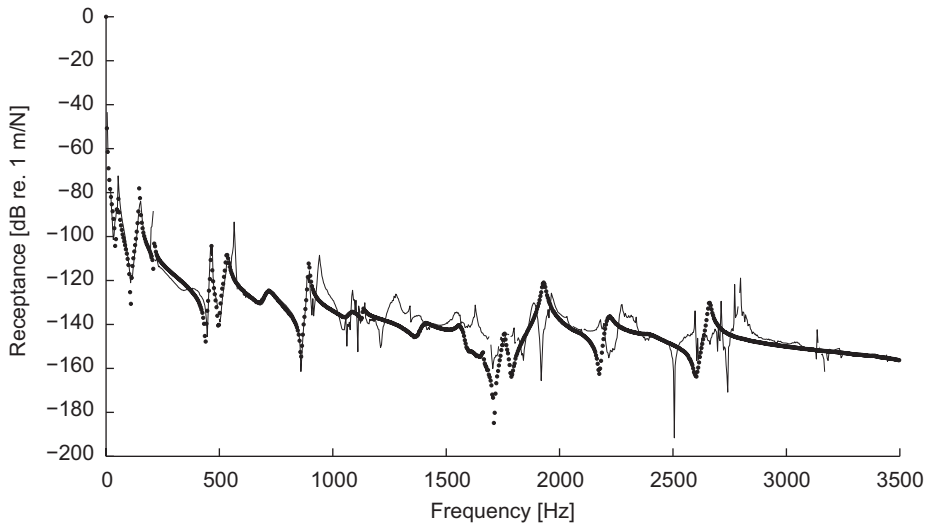

Fig. 14. Comparison of assembly FRFs ($S1_z/S1_z$)—direct solution. • Measured, — reconstructed.

Since the system is highly ill-conditioned, the parameters are non-unique solutions to an ill-conditioned problem. The identified stiffness, mass and viscous-damping matrices are given in Table 2 and the element of the dynamic stiffness matrix $\mathbf{Z}_j(1,1)$ is shown in Fig. 15. From the identified joint parameters and the substructure FRFs (measured and evaluated), the assembly FRFs were reconstructed. A comparison of the

Table 2
Identified stiffness, mass and hysteretic damping matrices of the joint

$$\mathbf{K} = \begin{bmatrix} -0.4143 & -0.2354 & -0.0023 & 0.0065 \\ -3.3131 & -1.2957 & 0.0430 & 0.1099 \\ 0.0585 & 0.0139 & -0.0054 & 0.0015 \\ 0.1925 & 0.0616 & -0.0048 & -0.0036 \end{bmatrix} \cdot 10^6$$

$$\mathbf{M} = \begin{bmatrix} -0.0277 & 0.0015 & 0.0003 & 0.0001 \\ -0.0155 & -0.0076 & 0.0002 & 0.0006 \\ 0.0000 & -0.0000 & -0.0000 & 0.0000 \\ 0.0014 & 0.0006 & -0.0000 & -0.0000 \end{bmatrix}$$

$$\mathbf{D} = \begin{bmatrix} 5.5274 & 0.6317 & -0.0262 & -0.0315 \\ -1.4468 & -2.7956 & 0.0006 & 0.3167 \\ 1.5624 & -0.3331 & -0.0271 & -0.0068 \\ 0.2614 & -0.0492 & -0.0127 & 0.0244 \end{bmatrix} \cdot 10^5$$

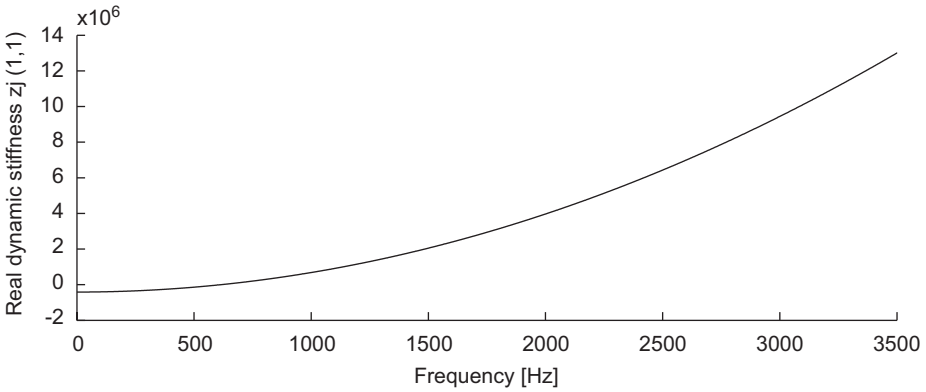

Fig. 15. Identified dynamic stiffness $\mathbf{Z}_j(1,1)$—least-squares solution of Eq. (14).

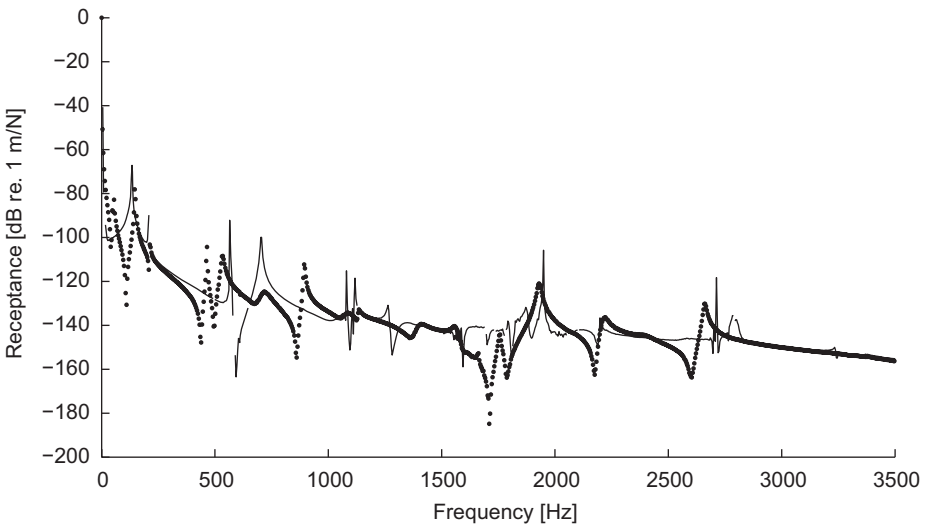

Fig. 16. Comparison of assembly FRFs ($S1_z/S1_z$)—least-squares solution. • Measured, — reconstructed.

measured and the reconstructed assembly receptances is given in Fig. 16. Although there are, in general, large discrepancies between the measured and reconstructed receptances in Fig. 16, some resonant frequencies are still correctly predicted by the reconstructed solution.

4. Conclusions

In this work, Ren and Beards' [4] joint-identification theory was extended to RDOFs. The validity of the proposed method was tested numerically and experimentally. From the numerical example it is evident that the exclusion of the RDOFs in the identification process leads to erroneous results.

Through numerical testing it became apparent that the numerical errors, as a consequence of system singularities, are the main reason for the erroneous results. The singularity problems can be reduced by an appropriate weighting of the equations, but they cannot be removed completely. Another possibility for solving these problems is the elimination of the linearly dependent equations from the whole system of equations. However, this task should be done with great caution, because important information about the system can be lost in this way.

Receptances related to joint coordinates and RDOFs are very difficult to measure. In this work an alternative solution to this problem was investigated. According to Ref. [2], unmeasured FRFs were estimated using the substructure FE model and measured FRF data. In contrast to similar methods [8,13], in our case the FRF data from the accurately calibrated FE model were not used directly in the identification process. However, these data were used for the estimation of the unmeasured FRFs. This approach also makes possible the identification of the damping in the joint.

Although the system was ill-conditioned, some useful results were obtained in the low-frequency range. The direct solution on a frequency-by-frequency basis gives very good results in the frequency range from 0 to 900 Hz.

Since a non-parametric model of the joint was used in the joint identification, and due to the nature of the least-squares approach, we get a non-physical solution, in general. However, this solution can still be used for a prediction of the assembly response in the frequency domain or as a starting value for the updating process.

It must be stressed that the MDOF system is a discrete system, while the beam is a continuum in nature. In the real world materials are not ideally homogeneous and isotropic, and therefore deriving a parametrical model of the joint is a very difficult task.

Appendix A

Eq. (13) for the identification of the dynamic stiffness matrix of the joint $\mathbf{Z}_j$ is appropriate for the numerical tests only. An alternative form of Eq. (13) is presented, which is more convenient for practical applications.

Rearranging Eq. (11) leads to

$$\begin{bmatrix} \mathbf{TT}_{nj} & \mathbf{TR}_{nj} \\ \mathbf{TT}_{jj} & \mathbf{TR}_{jj} \\ \mathbf{RT}_{jj} & \mathbf{RR}_{jj} \end{bmatrix} \left(\mathbf{I} + \mathbf{Z}_j \begin{bmatrix} \mathbf{TT}_{bb} & \mathbf{TR}_{bb} \\ \mathbf{RT}_{bb} & \mathbf{RR}_{bb} \end{bmatrix} \right) = \begin{bmatrix} \mathbf{TT}_{ab} & \mathbf{TR}_{ab} \\ \mathbf{TT}_{bb} & \mathbf{TR}_{bb} \\ \mathbf{RT}_{bb} & \mathbf{RR}_{bb} \end{bmatrix} \tag{A.1}$$

and furthermore

$$\begin{bmatrix} \mathbf{TT}_{nj} & \mathbf{TR}_{nj} \\ \mathbf{TT}_{jj} & \mathbf{TR}_{jj} \\ \mathbf{RT}_{jj} & \mathbf{RR}_{jj} \end{bmatrix} \mathbf{Z}_j \begin{bmatrix} \mathbf{TT}_{bb} & \mathbf{TR}_{bb} \\ \mathbf{RT}_{bb} & \mathbf{RR}_{bb} \end{bmatrix} = \begin{bmatrix} \mathbf{TT}_{ab} & \mathbf{TR}_{ab} \\ \mathbf{TT}_{bb} & \mathbf{TR}_{bb} \\ \mathbf{RT}_{bb} & \mathbf{RR}_{bb} \end{bmatrix} - \begin{bmatrix} \mathbf{TT}_{nj} & \mathbf{TR}_{nj} \\ \mathbf{TT}_{jj} & \mathbf{TR}_{jj} \\ \mathbf{RT}_{jj} & \mathbf{RR}_{jj} \end{bmatrix}. \tag{A.2}$$

Eq. (13) can also be rearranged in the form

$$\begin{bmatrix} \mathbf{TT}_{aa} - \mathbf{TT}_{nn} \\ \mathbf{TT}_{ba} - \mathbf{TT}_{jn} \\ \mathbf{RT}_{ba} - \mathbf{RT}_{jn} \end{bmatrix} \begin{bmatrix} \mathbf{TT}_{ba} \\ \mathbf{RT}_{ba} \end{bmatrix}^{+} = \begin{bmatrix} \mathbf{TT}_{nj} & \mathbf{TR}_{nj} \\ \mathbf{TT}_{jj} & \mathbf{TR}_{jj} \\ \mathbf{RT}_{jj} & \mathbf{RR}_{jj} \end{bmatrix} \mathbf{Z}_j, \tag{A.3}$$

where $[]^+$ stands for pseudo-inverse [9]. Substituting Eq. (A.3) into Eq. (A.2) yields

$$\begin{bmatrix} \mathbf{TT}_{aa}-\mathbf{TT}_{nn} \\ \mathbf{TT}_{ba}-\mathbf{TT}_{jn} \\ \mathbf{RT}_{ba}-\mathbf{RT}_{jn} \end{bmatrix} \begin{bmatrix} \mathbf{TT}_{ba} \\ \mathbf{RT}_{ba} \end{bmatrix}^{+} \begin{bmatrix} \mathbf{TT}_{bb} & \mathbf{TR}_{bb} \\ \mathbf{RT}_{bb} & \mathbf{RR}_{bb} \end{bmatrix} = \begin{bmatrix} \mathbf{TT}_{ab} & \mathbf{TR}_{ab} \\ \mathbf{TT}_{bb} & \mathbf{TR}_{bb} \\ \mathbf{RT}_{bb} & \mathbf{RR}_{bb} \end{bmatrix} - \begin{bmatrix} \mathbf{TT}_{nj} & \mathbf{TR}_{nj} \\ \mathbf{TT}_{jj} & \mathbf{TR}_{jj} \\ \mathbf{RT}_{jj} & \mathbf{RR}_{jj} \end{bmatrix}. \tag{A.4}$$

Rearranging Eq. (A.4) as

$$\begin{bmatrix} \mathbf{TT}_{nj} & \mathbf{TR}_{nj} \\ \mathbf{TT}_{jj} & \mathbf{TR}_{jj} \\ \mathbf{RT}_{jj} & \mathbf{RR}_{jj} \end{bmatrix} = \begin{bmatrix} \mathbf{TT}_{ab} & \mathbf{TR}_{ab} \\ \mathbf{TT}_{bb} & \mathbf{TR}_{bb} \\ \mathbf{RT}_{bb} & \mathbf{RR}_{bb} \end{bmatrix} - \begin{bmatrix} \mathbf{TT}_{aa}-\mathbf{TT}_{nn} \\ \mathbf{TT}_{ba}-\mathbf{TT}_{jn} \\ \mathbf{RT}_{ba}-\mathbf{RT}_{jn} \end{bmatrix} \begin{bmatrix} \mathbf{TT}_{ba} \\ \mathbf{RT}_{ba} \end{bmatrix}^{+} \begin{bmatrix} \mathbf{TT}_{bb} & \mathbf{TR}_{bb} \\ \mathbf{RT}_{bb} & \mathbf{RR}_{bb} \end{bmatrix} \tag{A.5}$$

and substituting into Eq. (13) leads to

$$\begin{bmatrix} \mathbf{TT}_{aa}-\mathbf{TT}_{nn} \\ \mathbf{TT}_{ba}-\mathbf{TT}_{jn} \\ \mathbf{RT}_{ba}-\mathbf{RT}_{jn} \end{bmatrix} = \left\{ \begin{bmatrix} \mathbf{TT}_{ab} & \mathbf{TR}_{ab} \\ \mathbf{TT}_{bb} & \mathbf{TR}_{bb} \\ \mathbf{RT}_{bb} & \mathbf{RR}_{bb} \end{bmatrix} - \begin{bmatrix} \mathbf{TT}_{aa}-\mathbf{TT}_{nn} \\ \mathbf{TT}_{ba}-\mathbf{TT}_{jn} \\ \mathbf{RT}_{ba}-\mathbf{RT}_{jn} \end{bmatrix} \cdot \begin{bmatrix} \mathbf{TT}_{ba} \\ \mathbf{RT}_{ba} \end{bmatrix}^{+} \begin{bmatrix} \mathbf{TT}_{bb} & \mathbf{TR}_{bb} \\ \mathbf{RT}_{bb} & \mathbf{RR}_{bb} \end{bmatrix} \right\} \mathbf{Z}_j \begin{bmatrix} \mathbf{TT}_{ba} \\ \mathbf{RT}_{ba} \end{bmatrix}. \tag{A.6}$$

References

[1] R.A. Ibrahim, C.L. Pettit, Uncertainties and dynamic problems of bolted joints and other fasteners, *Journal of Sound and Vibration* 279 (2005) 857–936.

[2] K.T. Yang, Y.S. Park, Join structural parameter idenitfication using a subset of frequency response function measurement, *Mechanical Systems and Signal Processing* 7 (1993) 509–530.

[3] J.S. Tsai, Y.F. Chou, The identification of dynamic characteristics of a single bolt joint, *Journal of Sound and Vibration* 125 (1988) 487–502.

[4] Y. Ren, C.F. Beards, Identification of joint properties of a structure using FRF data, *Journal of Sound and Vibration* 186 (1995) 567–587.

[5] W. Liu, Structural Dynamic Analysis and Testing of Coupled Structures, PhD Thesis, Imperial College of Science, Technology and Medicine, London, 2000.

[6] Y. Ren, C.F. Beards, Identification of effective linear joints using coupling and joint identification techniques, *Journal of Vibration and Acoustics* 120 (1998) 331–338.

[7] Y. Ren, C.F. Beards, On the nature of FRF joint identification technique, *Proceedings of the 11th International Modal Analysis Conference*, Florida, USA, 1993, pp. 473–478.

[8] T. Yang, H.S. Fan, S.C. Lin, Joint stiffness identification using FRF measurements, *Computers and Structures* 81 (2003) 2549–2556.

[9] N.M. Maia, J.M.M. Silva, *Theoretical and Experimental Modal Analysis*, Wiley, New York, 1997.

[10] Y. Ren, The Analysis and Identification of Friction Joint Parameters in the Dynamic Response of Structures, PhD Thesis, Imperial College of Science, Technology and Medicine, London, 1992.

[11] G.W. Skingle, Structural Dynamic Modification using Experimental Data, PhD Thesis, Imperial College of Science, Technology and Medicine, London, 1989.

[12] W. Liu, D.J. Ewins, The importance assessment of RDOF in FRF coupling analysis, *Proceedings of the 17th International Modal Analysis Conference*, Florida, USA, 1999, pp. 1481–1487.

[13] W. Liu, D.J. Ewins, Substructure synthesis via elastic media, *Journal of Sound and Vibration* 257 (2002) 361–379.